Check for updates

Received: 7 October 2022 | Accepted: 29 December 2022

DOI: 10.1002/pamm.202200199

Modeling and numerical simulation of flow processes of wood-polymer composites

Fabian Liese[1,*] and **Olaf Wünsch**[1]

[1] Institute of Mechanics, Chair of Fluid Mechanics, University of Kassel, D-34125 Kassel

The combination of natural fibers and polymers is finding expanding application in a range of industrial branches, and knowledge of the material behavior is essential for further improving the products and the processing procedure. In this work, the material behavior of wood-polymer composites (WPC) will be modeled and numerical simulations will be used to investigate the flow behavior. By means of rheological measurements, a shear thinning flow behavior of the composite can be determined, which is also often taken into account in the numerical simulation of WPC processing tools. Increasing shear viscosity and a formation of a yield point with increasing wood content can be observed. However, in addition to the shear-dominant deformation states, noticeable strain deformations also occur due to cross-sectional changes. In order to experimentally investigate and model the behavior of WPC under strain, this work involves measurements on hyperbolic dies in which a uniaxial strain state is present and extensional viscosity can be derived from this. Different boundary conditions such as noSlip, navierSlip and full slip are investigated in the simulations. In addition, during the extrusion of WPC, wall shear stresses of about 0.1 MPa and above can be observed. Measurements in a high-pressure capillary rheometer allow the wall slip velocity to be measured as a function of the wall shear stress at different wood contents. The wall slip behavior is modeled and taken into account accordingly as a boundary condition in the numerical simulations using OpenFOAM [8].

© 2023 The Authors. *Proceedings in Applied Mathematics & Mechanics* published by Wiley-VCH GmbH.

1 Introduction

The market for wood-polymer composites has been growing for years, so that the time- and cost-efficient numerical design of processing tools is becoming increasingly important. For the use of numerical methods the material behavior is necessary, whereby the determination of the shear viscosity as well as its implementation is common. In addition, wall slip can occur above certain wall shear stresses, which is not considered in many numerical simulations. In addition to shear flow, extensional flow also occurs, the flow behavior of which is much more difficult to determine. The semi-hyperbolic die was first proposed by Everage and Ballmann [1] as a geometry to generate a uniaxial strain state and derive the extensional viscosity from it. Due to the special shape of the cross-sectional contraction, a constant strain rate is present in the core region of the die under wall slip or under high Reynolds numbers [2], [3]. In the present work, flow behavior is modeled on the basis of rheological investigations and numerical simulations are used to compare the flow of a hyperbolic die with experimental data.

2 Material modeling

In the material modeling, deformation variables are first defined and then the modeling of shear viscosity and wall slip behavior of HDPE 259 with different wood content is discussed. The deformation rate tensor $\mathbf{D} = \frac{1}{2}\left(\nabla\mathbf{v} + \nabla\mathbf{v}^T\right)$ is composed of the gradient of the velocity vector. From the invariants of the deformation rate tensor, deformation parameters such as the shear rate $\dot{\gamma}$, the uniaxial strain rate $\dot{\epsilon}$ and the parameter κ can be derived. On the basis of κ, a distinction can be made between pure shear and uniaxial or biaxial strain. For the calculation of the extra stress tensor $\mathbf{T}$ the approach for generalized Newtonian fluids is used. In addition, the flow can be assumed to be steady state, incompressible and isothermal.

Table 1: Deformation parameters and stress calculation

Invariants of $\mathbf{D}$	Deformation parameters	Stress calculation
$I_D = \mathrm{tr}(\mathbf{D}) = 0$	$\dot{\gamma} = \sqrt{-4II_D}$	$\mathbf{T} = \varphi_1(II_D, III_D)\mathbf{D}$
$II_D = -\frac{1}{2}\mathrm{tr}(\mathbf{D}^2)$	$\dot{\epsilon}_u = -3\frac{III_D}{II_D}$	$\varphi_1 = 2\eta(\dot{\gamma})$
$III_D = \det(\mathbf{D})$	$\kappa = \frac{III_D}{(-II_D)^{\frac{3}{2}}}$	

To determine the shear viscosity, rheological tests are performed in a rotational rheometer using a plate-plate setup for small shear rates and a capillary rheometer for large shear rates. The wood content varies between 30 % - 70 % wood content and the results shown are for 190 °C. Figure 1 shows the shear thinning viscous behavior of the composite. Between 30 % and 50 %, the zero viscosity increases by about a decade and a yield point is formed at 70 % wood content.

* Corresponding author: e-mail fluiddynamics@uni-kassel.de, phone +49 561 804 3252, fax +49 561 804 2720

This is an open access article under the terms of the Creative Commons Attribution-NonCommercial-NoDerivs License, which permits use and distribution in any medium, provided the original work is properly cited, the use is non-commercial and no modifications or adaptations are made.

© 2023 The Authors. *Proceedings in Applied Mathematics & Mechanics* published by Wiley-VCH GmbH.

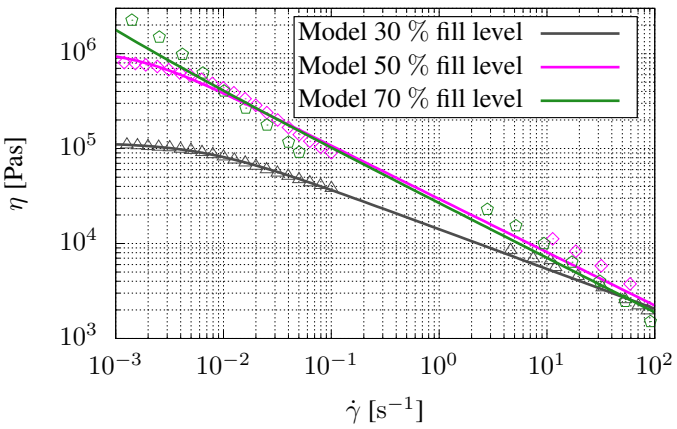

Fig. 1: Shear viscosity measurements (symbols) and model (lines) with different fill level of wood

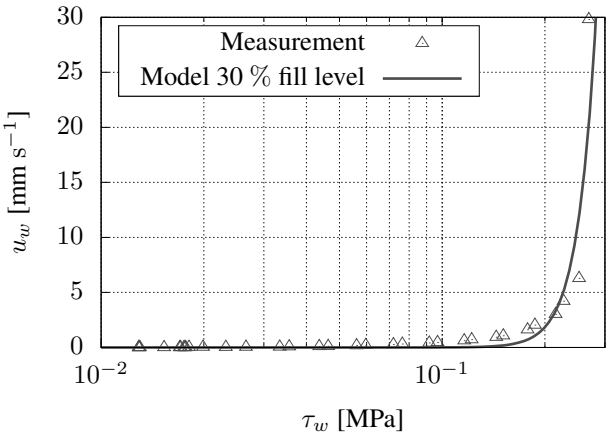

Fig. 2: Wall slip measurements (symbols) and model (lines) with 30 % fill level of wood

A Carreau-Yasuda model disregarding η_∞ is used to model this flow behavior at 30 % wood content:

$$\eta(\dot{\gamma}) = \eta_0 \left[1 + (\lambda|\dot{\gamma}|)^\alpha\right]^{\frac{n-1}{\alpha}} . \tag{1}$$

In addition to the nonlinear viscous flow law, wall slip can also play an important role in the processing of polymer melts. Due to the alignment of the molecular chains, at certain shear stress the fluid can no longer stick to the wall and begins to slip [4], [5]. Figure 2 shows measured data of WPC with 30 % wood content at 190 °C, obtained with the capillary rheometer using the Mooney method [6] with two dies of the same L/D and different length. A noticeable wall slip velocity is formed from wall shear stresses of about 0.1 - 0.2 MPa. The wall slip velocity $u_w(\tau_w)$ is modeled by a nonlinear navier slip model [7]:

$$u_w(\tau_w) = k|\tau_w|^m. \tag{2}$$

The implementation of the nonlinear shear viscosity and the wall shear stress-dependent wall slip velocity into the numerical model in OpenFOAM as well as the comparison to the experimental data is described in the next chapter 3.

3 Numerical simulations

For a more detailed flow investigation, a combination of a hyperbolic die and a following pipe with constant cross-section is manufactured, which can be seen in Fig. 3. Via a capillary rheometer, the molten WPC material is pressed through the geometry with a defined volume flow. The pressure is recorded at the inlet to the hyperbolic die with $p1$ and at the outlet of the hyperbolic die with $p2$. The temperature in the inserted die is measured at two points and is used to control the amount of external heat. A creeping flow with Re $\ll 1$ is present.
A velocity-inlet and pressure-outlet are defined as boundary conditions for the numerical simulations. To implement the wall shear stress dependent slip velocity, the rheoTool of OpenFOAM [8] is used:

$$\begin{aligned} {\mathbf{v}_w}^{t+dt} &= (1 - URF){\mathbf{v}_w}^t + URF\left(-k|\boldsymbol{\tau}_w|^m \frac{\boldsymbol{\tau}_w}{|\boldsymbol{\tau}_w|^m}\right), \\ \boldsymbol{\tau}_w &= \mathbf{T}_w \cdot \mathbf{n} - [(\mathbf{T}_w \cdot \mathbf{n})]\mathbf{n}. \end{aligned} \tag{3}$$

The velocity vector on the wall at the new time step ${\mathbf{v}_w}^{t+dt}$ is obtained with underrelaxation factor URF and the normal vector $\mathbf{n}$ by equation (3).

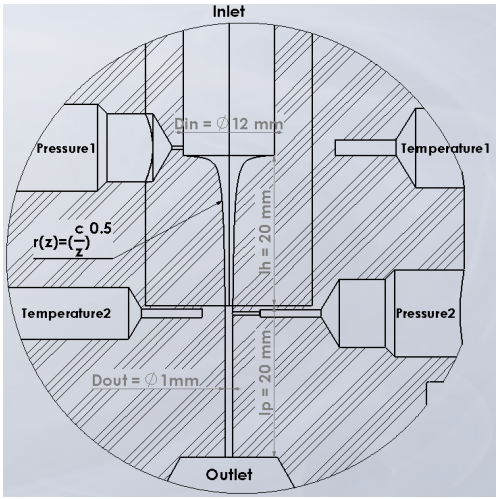

Fig. 3: Design of the experimental setup with hyperbolic die, pipe and sensors

© 2023 The Authors. *Proceedings in Applied Mathematics & Mechanics* published by Wiley-VCH GmbH.

3.1 Pipe flow

In this subsection, the pipe flow in the constant cross-section with diameter $D_{\text{out}} = 1$ mm over the length of $l_{\text{p}} = 20$ mm is investigated. The pressure drop of the pipe flow corresponds to the pressure difference between the sensor $p2$ and the outlet where ambient pressure is present.

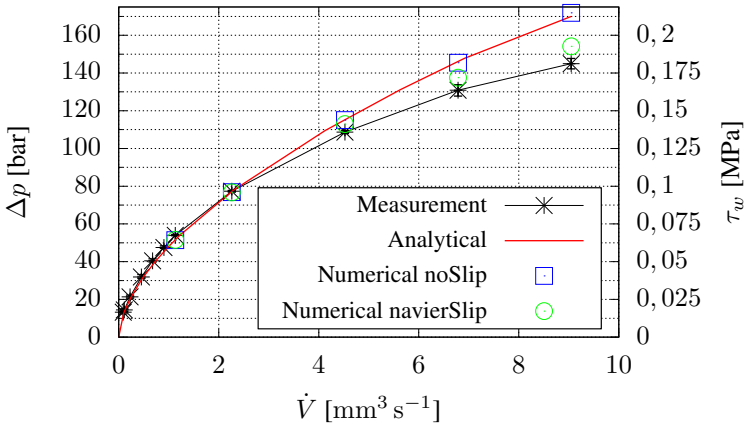

Fig. 4: $\Delta p(\dot{V})$ and $\tau_w(\dot{V})$ measurements, analytical and numerical with noSlip and navierSlip boundary condition in pipe flow

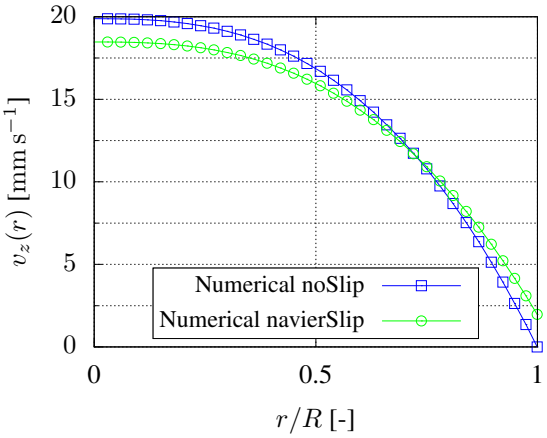

Fig. 5: Velocity profile in pipe flow with navierSlip and noSlip boundary

Figure 4 shows the pressure drop Δp as well as the wall shear stress τ_w as a function of the volume flow $\dot{V}$. The experimental data show a degressive increase in pressure drop with increasing volume flow, which is to be expected for shear thinning viscosity. In red is shown an analytical solution from [9] for the Carreau-Yasuda model for pipe flows and in blue some numerical results with noSlip boundary condition. There is good agreement between the analytical and numerical results over the entire volume flow range. For wall shear stresses smaller than 0.1 MPa, the experimental data also show good agreement with the analytical and numerical solution. For wall shear stresses greater than 0.1 MPa, the increase in pressure drop is smaller in the experimental data than in the analytical solution. This can be explained by the wall slip effect. The numerical data with the navierSlip boundary condition by equation (3) can reproduce this effect and show a relatively good agreement with the experimental data, even if the pressure drop is somewhat overestimated in the simulation.

The influence of wall slip on the simulated velocity profile can be seen in Fig. 5. There, the velocity in axial direction v_z is plotted versus the normalized radius r/R. In blue is the profile for the noSlip boundary condition, where the velocity at the wall is zero and the profile for shear thinning viscosity is formed. In green is shown the velocity profile with the navierSlip boundary condition at a volume flow of 9 $\text{mm}^3\ \text{s}^{-1}$, where a wall slip velocity $u_w = 1.97\ \text{mm}\ \text{s}^{-1}$ is formed. The shear rate at the wall decreases accordingly and the maximum velocity at the center of the pipe is also lower, so that the pressure drop is reduced.

3.2 Hyperbolic die

The hyperbolic die can be used to generate a uniaxial deformation state under full wall slip. This will be investigated experimentally and numerically, although complete wall slip is not present in the experiments. This will be carried out in further work. The inlet radius of the die of $R_{\text{in}} = 6$ mm corresponds to the radius of the rheometer and from $z = 0$ the contour of the hyperbolic die over the length $l_h = 20$ mm is given by the function

$$r(z) = \sqrt{\frac{c}{z}}. \tag{4}$$

Here $c = r^2(z)z = 5\ \text{mm}^3$ is a constant and z is the axial coordinate. From preliminary investigations, the outlet diameter of $R_{\text{out}} = 0.5$ mm showed a good compromise between the requirement that the diameter of the filler wood is significantly smaller than that of the flow channel and the achievement of large wall shear stresses. The area ratio between inlet and outlet gives the Hencky strain $\epsilon_h = \ln\left(\frac{{R_{\text{in}}}^2}{r(z)^2}\right) = \ln\left(\frac{z}{z_{\text{in}}}\right)$, which here has a limit value of 5. The influence of ϵ_h on the stress component τ_{rz} is discussed in Fig. 6. Under the condition of wall slip, for the uniaxial strain state the radial velocity is $v_r = -\frac{1}{2}\dot{\epsilon}r$ and the axial velocity is $v_z = \dot{\epsilon}z$. From the axial velocity component follows the volume flow and conveniently converted according to the strain rate follows:

$$\dot{\epsilon} = \frac{\dot{V}}{\pi r^2(z)z} = \frac{\dot{V}}{\pi c}. \tag{5}$$

© 2023 The Authors. *Proceedings in Applied Mathematics & Mechanics* published by Wiley-VCH GmbH.

The extensional viscosity η_E generally results from the first normal stress difference and the strain rate:

$$\eta_E = \frac{\tau_{zz} - \tau_{rr}}{\dot{\epsilon}}. \tag{6}$$

The strain rate can be determined by equation (5) from the volume flow. To determine the stress components τ_{zz} and τ_{rr} from the measured pressure drop, the equation of motion in the axial direction is first established for isothermal, incompressible, steady-state, axially symmetric flows, neglecting the volume force:

$$\rho\left(v_z\frac{\partial v_z}{\partial z} + v_r\frac{\partial v_z}{\partial r}\right) = -\frac{\partial p}{\partial z} + \frac{\partial \tau_{zz}}{\partial z} + \frac{1}{r}\frac{\partial}{\partial r}(r\tau_{rz}). \tag{7}$$

The velocity and stress field in the present flow is independent of the φ-component, but of the radial and axial components. Under wall slip $\partial v_z/\partial r = 0$ can be assumed and introducing the outward normal vector $\mathbf{n}$ the following boundary condition can be assumed at the wall ($r = R$) with $\mathbf{T}\cdot\mathbf{n} = \mathbf{0}$. Hence, with the components of $\mathbf{n}$ in z and r direction, the following equation can be established for τ_{rz} by [10], [11]:

$$\tau_{rz}(R) = -\frac{n_z}{n_r}\tau_{zz}(R) = -\frac{dr}{dz}\tau_{zz} \tag{8}$$

Thus, the shear stress τ_{rz} depends on τ_{zz} via the factor dr/dz. Therefore, this geometric factor is investigated in more detail. For the manufactured hyperbolic die, Fig. 6 plots the derivative dr/dz of the function (4) and, on the second axis, the Hencky strain ϵ_h versus the coordinate z. The geometric quantities are $z_{\text{in}} = 0.13889$ mm, $R_{\text{in}} = 6$ mm and $R_{\text{out}} = 0.5$ mm. The change in radius r over the coordinate z asymptotically approaches 0 and has fallen below a value of 0.1 at a length of 5 mm.

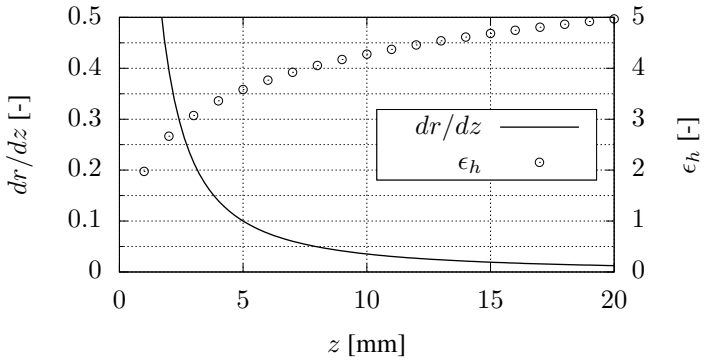

Fig. 6: $\epsilon_h(z)$ and $dr/dz(z)$ of hyperbolic die

Thus, according to equation (8), it can be said that the stress component τ_{rz} has a relevant influence only in the foremost region of the die. The Hencky strain at this point is 3.6, which is consistent with [11]. By integrating the equation (7) over z and the condition of small Reynolds numbers, which allows neglecting inertial forces, and neglecting τ_{rz}, the stress τ_{zz} can be assigned to the pressure drop Δp over the die length:

$$\tau_{zz} = -\Delta p. \tag{9}$$

The stress component τ_{rr} is often set to zero in the literature [3]. When setting up the equation of motion in the radial direction, it quickly becomes apparent that the second normal stress difference must be determined [2], the experimental detection of which poses considerable challenges. Thus, the simplification of $\tau_{rr} = \tau_{\varphi\varphi} = 0$ is used. Therefore, it follows from equation (6) and equation (9) for steady state or so called strain averaged extensional viscosity:

$$\eta_E = \frac{\tau_{zz} - \tau_{rr}}{\dot{\epsilon}} = \frac{-\Delta p}{\dot{\epsilon}\epsilon}. \tag{10}$$

Thus, with the experimental setup, the strain averaged extensional viscosity can be calculated from the measured pressure drop along the hyperbolic die and the volume flow converted to the strain rate.

Figure 7 shows the pressure drop $\Delta p = p_1 - p_2$ across the hyperbolic die as a function of volume flow. The experimental data again show a degressive decrease of the pressure drop with increasing volume flow, although the simulated pressure drops are always significantly lower than the experimental data. The influence of wall slip with the navierSlip boundary condition is negligible due to the lower wall shear stress over most of the die. Only the shear viscosity is implemented in the numerical model, so the difference between experimental and numerical data must be related to other effects, which will be investigated by numerical and experimental methods.

To calculate the extensional viscosity from the experimental and numerical data, equation (10) is used, resulting in the extensional behavior $\eta_{E,\text{Measurement}}$ with very large extensional viscosities in Fig. 8. Since there is no wall slip in the present experiment, there is a superposition of shear and strain. To identify the pressure drop resulting from strain deformations, the experimentally determined pressure drop $\Delta p_{\text{Measurement}}$ is subtracted by the simulated pressure drop $\Delta p_{\text{num,shear}}$. The simulated pressure drop results only from the shear viscosity, so that the corrected extensional viscosity $\eta_{E,\text{Corrected}}$ depending

© 2023 The Authors. *Proceedings in Applied Mathematics & Mechanics* published by Wiley-VCH GmbH.

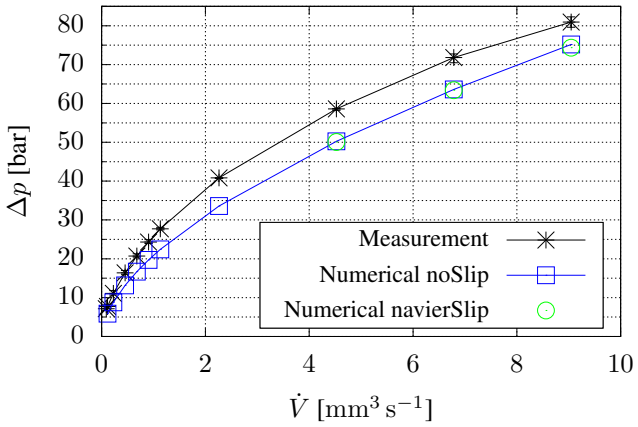

Fig. 7: Hyperbolic die flow $\Delta p(\dot{V})$ measurements and numerical

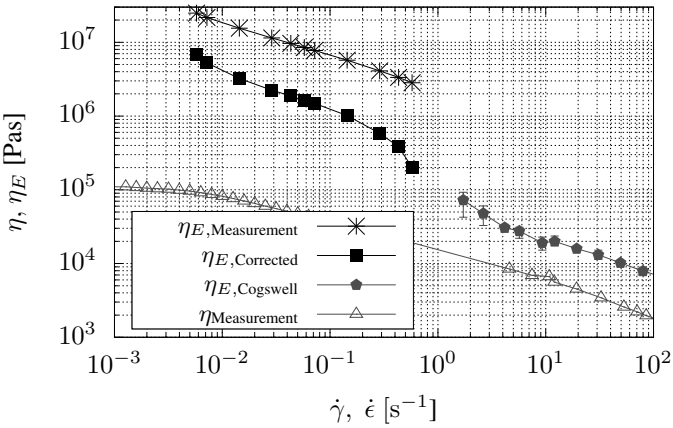

Fig. 8: Shear and extensional viscosity depending on deformation [12]

on $\Delta p_{\text{Measurement}} - \Delta p_{\text{num,shear}}$ can be approximately assigned to the pressure drop due to strain. The extensional viscosity as a function of strain rate is substantially reduced by this correction. Figure 8 also plots experimental data from a Cogswell model [12] resulting from the inlet pressure drop from additional measurements on the capillary rheometer. This extensional viscosity also shows strain-thinning behavior, which are of a similar order of magnitude to $\eta_{E,\text{Corrected}}$. The shear viscosity $\eta_{\text{Measurement}}$ is also plotted, showing very large Trouton ratios especially for small deformations.

In the numerical simulations, the influence of the different boundary conditions is shown, distinguishing between the boundary condition slip on the left side and noSlip on the right side. Figure 9 shows the κ value from table 1 and Fig. 10 shows the difference of the stress components $\tau_{zz} - \tau_{rr}$, which is used for an extensional viscosity calculation.

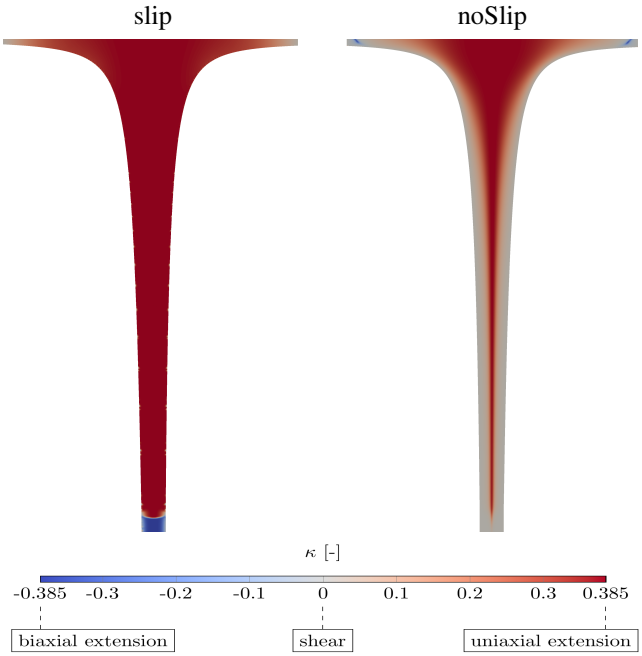

Fig. 9: Numerical κ-field in semi-hyperbolic die. Left slip, right noSlip

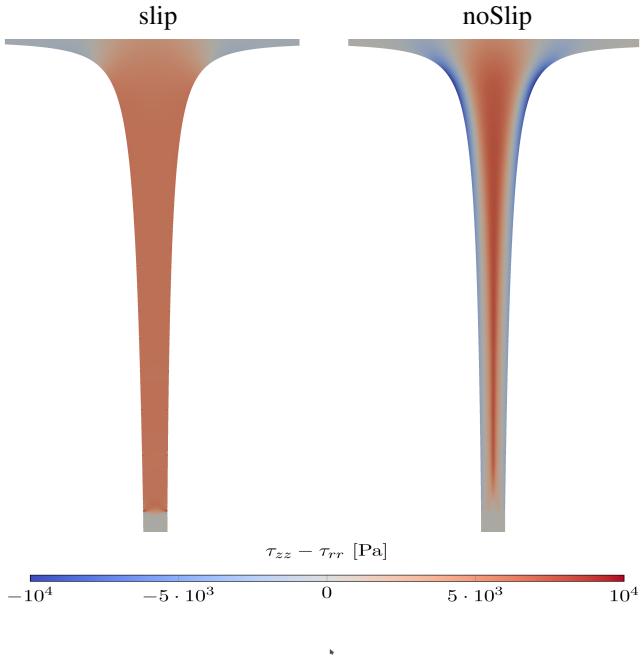

Fig. 10: Numerical $\tau_{zz} - \tau_{rr}$-field in semi-hyperbolic die. Left slip, right noSlip

The κ value can be used to visualize the deformation state present. For a value of 0, pure shear is present in gray, which is the case for the noSlip boundary condition in the constant cross-section pipe and near the wall of the hyperbolic die. Uniaxial strain is shown in red for a limit value of 0.385, which is the case for the slip boundary condition in the entire region of the hyperbolic die. For the noSlip boundary condition, uniaxial strain is present in the core region of the die.

The stress difference $\tau_{zz} - \tau_{rr}$ for calculating the extensional viscosity is shown in Fig. 10 for the two different boundary conditions. For the slip boundary condition, over most of the hyperbolic die, this diffenence is constant. The influence of τ_{rz} over the inlet region of the die, which was investigated in more detail in Fig. 6, is shown by a reduction of the stress difference $\tau_{zz} - \tau_{rr}$ in the inlet region. With the noSlip boundary condition on the right, the influence of shear on the stress near the wall can be clearly seen.

© 2023 The Authors. *Proceedings in Applied Mathematics & Mechanics* published by Wiley-VCH GmbH.

4 Results and discussion

For the design of WPC extrusion dies, knowledge about the material behavior is essential, which was investigated in this work for different flow conditions. The investigation in a pipe with constant diameter showed good agreement between experimental, analytical and numerical data for small wall shear stresses. Above wall shear stresses of 0.1 MPa, the experimental data show a clear reduction in pressure drop, which could be reproduced numerically with a navierSlip model. To determine the extensional viscosity, the flow on a hyperbolic die was investigated. The simulated pressure drops were significantly lower than the experimental data, which was attributed to the extensional viscosity. When the pressure drop is transferred to the extensional viscosity, the corrected values give reasonable agreement with data from a Cogswell model.
In further work, a lubricating film should be included into the experimental setup to suppress wall adhesion. In addition, the influence of the second normal stress difference should be investigated in more detail.

Acknowledgements Open access funding enabled and organized by Projekt DEAL.

References

[1] A. E. Everage and R. L. Ballmann, The extensional flow capillary as a new method for extensional viscosity measurement. Nature **273**, 213-215 (1978).
[2] D. F. James, G. M. Chandler and S. J. Armour, A converging channel rheometer for the measurement of extensional viscosity. Journal of Non-Newtonian Fluid Mechanics **35**, 421-443 (1990).
[3] J. R. Collier, O. Romanoschi and S. Petrovan, Elongational rheology of polymer melts and solutions. Journal of Applied Polymer Science **69**, 2357-2367 (1998).
[4] S. G. Hatzikiriakos, Wall slip of molten polymers. Progress in Polymer Science **37**, 624-643 (2012).
[5] V. Hristov, R. Takács and J. Vlachopoulos, Surface Tearing and Wall Slip Phenomena in Extrusion ofHighly Filled HDPE/Wood Flour Composites. Polymer Engineering and Science **46**, 1204-1214 (2006).
[6] M. Mooney, Explicit Formulas for Slip and Fluidity. Journal of Rheology **2**, 210-222 (1931).
[7] C. Fernandes et al., Implementation of partial slip boundary conditions in an open-source finite-volume-based computational library. Journal of Polymer Engineering **39**, 377-387 (2019).
[8] F. Pimenta and M. A. Alves, rheoTool (2022), p. 122.
[9] T. Sochi, Analytical solutions for the flow of Carreau and Cross fluids in circular pipes and thin slits. Rheologica Acta **54**, 745-756 (2015).
[10] D. G. Baird, and D. I. Collias Polymer Processing : Principles and Design (Wiley, New Jersey, 2014), p. 212.
[11] D. G. Baird and J. Huang, Elongational Viscosity Measurements Using a Semi-Hyperbolic Die. Applied Rheology **16**, 312-320 (2006).
[12] C. Kwag and J. Vlachopoulos, An assessment of cogswell's method for measurement of extensional viscosity. Polymer Engineering and Science **31**, 1015-1021 (1991).

© 2023 The Authors. *Proceedings in Applied Mathematics & Mechanics* published by Wiley-VCH GmbH.